Fuel Stratification Effects on Gasoline Compression Ignition with a Regular-Grade Gasoline on a Single-Cylinder Medium-Duty Diesel Engine at Low Load

Author, co-author (Do NOT enter this information. It will be pulled from participant tab in MyTechZone)

Affiliation (Do NOT enter this information. It will be pulled from participant tab in MyTechZone)

Abstract

Previous research studies have investigated a wide variety of gasoline compression ignition injection strategies and the resulting fuel stratification levels to maintain control over the combustion phasing, duration, and heat release rate. Previous gasoline compression ignition research at the US Department of Energy's Oak Ridge National Laboratory has shown that for a combustion mode with a low degree of fuel stratification, called "partial fuel stratification" (PFS), gasoline range fuels with anti-knock index values in the range of regular-grade gasoline (~87 anti-knock index or higher) provides very little controllability over the timing of combustion without significant boost pressures. On the contrary, heavy fuel stratification (HFS) provides control over combustion phasing but has challenges achieving low temperature combustion operation, which has the benefits of low NO_X and soot emissions, because of the air handling burdens associated with the required high exhaust gas recirculation rates. This work investigates HFS and PFS combustion, efficiency, and emissions performance on a single-cylinder, medium-duty engine with a regular-grade gasoline (91 research octane number) at 1,200 rpm, 4.3 bar, and 3.0 nominal gross indicated mean effective pressure operating points with boost levels similar to those in a medium-duty diesel application. Authority of combustion phasing with main injection timing sweeps for HFS and second injection timing sweeps and fuel split sweeps for PFS are shown. In addition, this work is discussed in the context of previous findings with a light-duty diesel platform, and next steps and future direction for this work are presented.

1 Introduction

Medium-duty (MD) and heavy-duty (HD) internal combustion engines are expected to continue to be the dominate propulsion system in the commercial truck sector for the foreseeable future. Recent studies forecasted that the on-road movement of freight will continue to use internal combustion engine powertrains as the dominant prime mover for many years. A summary of recent studies can be found from Reitz et al. [1]. Diesel engines are the prevalent engine type in the on-road commercial vehicle sector in the United States, and 82% of Class 4–8 MD-HD truck sales were diesel engine–based in 2019 [2]. For on-road MD-HD vehicle applications that meet the US Environmental Protection Agency 2017 emissions certification, engines can be approximately classified by bore size. For current on-road MD engines, bore sizes range from about 94 to 110 mm, and HD bore sizes are in the 114–137 mm range. These generalizations on bore size are not conclusive, but they help differentiate studies by application in conventional powertrains (i.e., not hybrid-electric configurations).

Although industry continues to make strides in improving efficiency, engine-out emissions, and tailpipe-out emissions with diesel technologies, there is a continued interest in being able to operate MD-HD engines on gasoline–boiling range fuels as a way to increase resilience in a quickly changing fuel market and to further improve emissions. Therefore, advancements in understanding of underlaying physical and chemical process governing engine efficiency and emissions formation continue to drive research and development for combustion processes such as gasoline compression ignition (GCI), which can include approaches that can be classified as low-temperature combustion (LTC).

LTC is broadly characterized by the simultaneous reduction of soot and NO_X while maintaining high fuel conversion efficiency. LTC is often referenced in terms of having the majority of the fuel-air charge outside the local equivalence ratio and temperature regions that support formation of soot and NO_X as illustrated in Figure 1. As with the ability to achieve LTC for combustion of diesel fuel through manipulation of injection timing and dilution, similar results can be achieved for GCI, resulting in either "conventional" or LTC operating modes.

The classification of different injection strategy approaches as a function of fuel-air stratification proposed by Dempsey et al. [3] helps characterize the opportunities and challenges of achieving LTC in practical engine systems. This conceptual model is illustrated in

Figure 2 with fully premixed and kinetically controlled modes such as homogeneous charge compression ignition (HCCI) on one end of the spectrum, and diesel-like mixing controlled compression ignition on the other end.

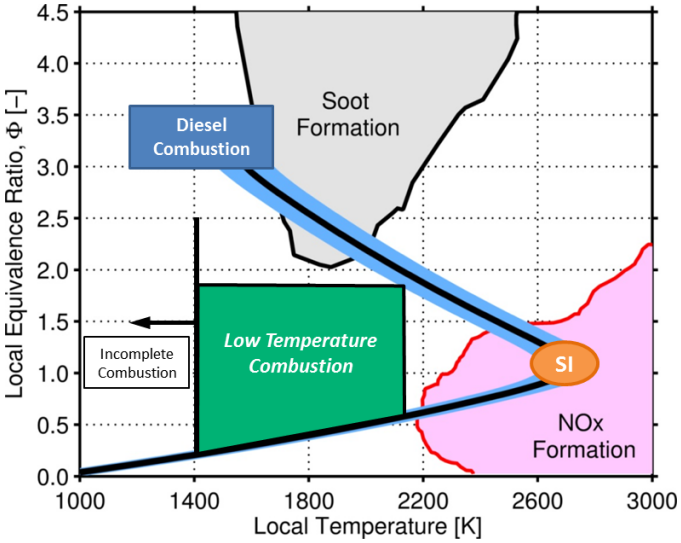

Figure 1. Illustration of LTC region avoiding zones where local conditions favor formation of NOx and soot emissions on a local equivalence ratio and local temperature (Phi-T) diagram with illustrative diesel and homogenous spark-ignition areas. (Modified with permission from Dempsey et al. [3].)

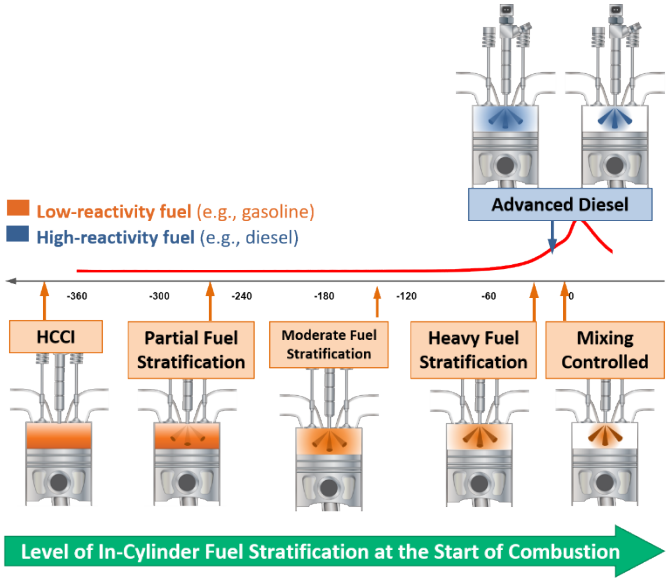

Figure 2. Conceptual model of fuel injection timing and fuel stratification with arrows representing notional centroid of quantity of fuel injected and level of fuel-air stratification. (Modified with permission from Dempsey et al. [4]).

Further examination of the two ends of this stratification spectrum—partial fuel stratification (PFS) on the kinetically controlled compression ignition side and heavy fuel stratification (HFS) on the mixing-controlled compression ignition side—is particularly useful in contextualizing opportunities and challenges for implementing GCI. PFS can use port fuel injection or very early direct injection during the intake stroke to create a nearly homogeneous charge of fuel and air. Subsequent direct injections occur during the compression stroke to create slight levels of fuel stratification to help create sequential autoignition events while maintaining near-zero levels of NO_X and soot emissions with more control authority than can be achieved with classical HCCI combustion. HFS uses a high level of fuel stratification similar to that of conventional diesel combustion (CDC) and typically features no fully premixed fuel, with direct injection(s) relatively close to top dead center (TDC) [13, 19]. HFS requires high amounts of exhaust gas recirculation (EGR) to achieve LTC operation. PFS with gasoline has been shown to provide very little controllability over the timing of combustion. On the other hand, HFS provides very linear and pronounced control over the timing of combustion. The Dempsey et al. study describes the challenges and opportunities for HFS and PFS strategies [3]. In both light-duty (LD) and MD-HD studies, many of the experimental GCI investigations have been conducted on diesel engine platforms with high-pressure direct injection fuel systems and with high geometric compression ratios.

Although many MD-HD GCI studies have investigated high-load operation and peak brake thermal efficiency along with requirements for full load range [4, 5], other studies have focused on the low-load operability of GCI. Overcoming challenges associated with low-load operation, including combustion stability and engine-out emissions, is critical for GCI implementation in production engines. In addition, cold-start emissions, emissions compliance, transient controls, and other real-world implementation elements are key performance elements that will also need to be addressed. Studies have looked at enabling technologies in MD-HD GCI engines, including changes in compression ratio and use of variable valve actuation to improve GCI performance by Zhang et al. [6], the use of glow plugs to assist the combustion process by Zhao et al. [7], and piston bowl geometry effects by Tang et al. [8].

Recent MD-HD research has included detailed studies on low-load GCI operation and the associated opportunities and challenges. Dec et al. [9] used a 102 mm bore single-cylinder research engine based on a Cummins B-series diesel engine with a range of different market-grade gasolines and varying amounts of ethanol to investigate the roles of changes in octane number and boost pressure in autoignition reactivity during PFS and HCCI GCI approaches. More recent studies on the same engine platform led by Lopez et al. [10] used an E10, 87 anti-knock index (AKI) gasoline, termed RD5-87, with and without a cetane enhancer (2-ethylhexyl nitrate) to evaluate the roles of reactivity, phi-sensitivity, and fuel-fraction split on control authority over combustion phasing.

Recent low-load GCI studies by Roberts et al. were conducted using a 107 mm bore diesel engine modified from a Cummins 6.7 L ISB as a single-cylinder engine [11]. The engine research platform was modified to have a port fuel injection system in addition to the high-pressure direct-injection fuel system and used an ~89 AKI gasoline with a lubricity additive with gasoline-diesel blends at a 2.0 bar gross indicated mean effective pressure (IMEPg) load at 1,200 rpm. The authors found that an EGR level of 50% was needed at an intake pressure of 139 kPa to meet their NO_X target of 1 g/kg-fuel, with additional EGR required at lower intake pressures for achieving the same NO_X target with the diesel–gasoline blends. The authors studied the NO_X emissions at minimum intake pressure for each of the fuels at the low load, using as much as 60% EGR.

Additional study by Babu, Roberts, and Kokjohn [12] investigated the role of gasoline fuel properties, namely research octane number (RON) and octane sensitivity, on stability of operation, and a recent study by Chung et al. [13] at Southwest Research Institute used a 131 mm bore single-cylinder research engine based on a 2017 Volvo

D13 13 L diesel engine with both a stepped-lip and “wave” piston with a pump-grade E10 (10% ethanol by volume) with 500 ppm of a lubricity additive. The study investigated the role of fuel stratification at low loads via injection timing sweeps from −120° after TDC (ATDC) toward TDC at 4.5 bar IMEPg at 1,000 and 1,200 rpm. A sharp increase in normalized NO_X was observed as injection timing approached TDC. Moderate amounts of EGR were used to achieve a 5–6 g/kW-hr NO_X level with approximately 47%–48% gross indicated thermal efficiency (ITEg) at low loads. Further discussion on foundational work in GCI in MD-HD engines can be found in several papers that were summarized by Dempsey et al. [4].

There have been studies of GCI with lower-octane gasoline-range fuels that are well below the minimum octane requirements for motor gasoline [14, 15, 16]. The use of gasoline-range fuels in RON > 60 but less than market grade gasoline were covered by Kalghatgi [17]. The advantage for research into GCI with gasoline-range fuels that fall into what would be considered a market-available range in the United States such that the AKI is greater than 87 for “regular grade” is that the fuel already exists in the market with current infrastructure with key performance requirements set forth in ASTM D4814−21 [18].

Previous GCI research by Dempsey et al. [16] conducted using a multi-cylinder, LD diesel engine research platform across the range of fuel-air stratification levels was noted earlier. This work demonstrated that PFS with gasoline range fuels with RON values in the range of market-grade gasoline (~87 AKI or higher) provides very little controllability over the timing of combustion without significant boost pressures. By contrast, HFS provides control over combustion phasing but has challenges achieving LTC operation due to the air handling burdens associated with the high EGR rates that are required to reduce NO_X emissions to near-zero levels.

This scoping study investigates HFS and PFS combustion, efficiency, and emissions performance on a single-cylinder MD engine with a market-grade gasoline (91 RON) at 1,200 rpm, 3.0 bar, and 4.3 bar IMEPg operating points with intake pressure and temperature levels similar to those in typical on-road MD diesel applications. The LTC operational requirements for HFS and PFS GCI operating strategies and control authority with the MD platform are investigated. Authority of combustion phasing with injection timing sweeps for HFS and with second injection timing sweeps and fuel split sweeps for PFS is also investigated. A final comparison of PFS and HFS with a CDC case is also presented. Figure 3 shows the stratification ends being investigated in this work, including the objectives for each end with illustrative fuel injection strategies.

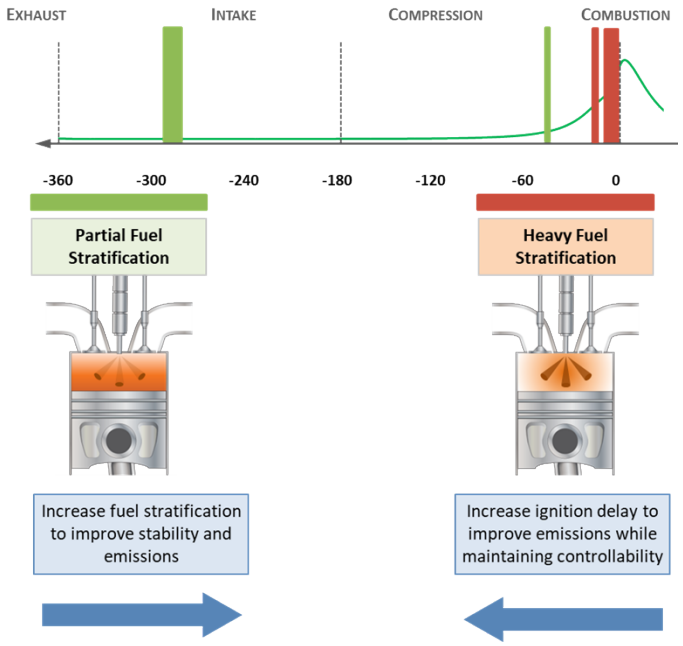

Figure 3. PFS and HFS injection strategies and objectives for challenges for achieving high-efficiency LTC operation with minimal HC and CO emissions.

2 Methodology

The following sections summarize the engine configuration, measurement and data acquisition systems, fuel, and data analysis approach.

2.1 Experimental Setup

The engine used for this study was a 6.7 L Cummins ISB diesel engine that was modified to operate as a single-cylinder engine. Five of the cylinders were disabled, and custom intake and exhaust manifolds were used. The combustion chamber geometry was not modified from the stock configuration. The stock engine geometric specifications are shown in Table 1. Figure 4 shows the overall engine and fuel system layout.

Table 1. Engine specifications for a Cummins 6.7 L ISB diesel engine used for GCI experiments.

Parameter	Value
Number of cylinders [-]	1
Bore [mm]	107
Stroke [mm]	124
Connecting rod length [mm]	145.4
Compression ratio [-]	20:1
Total displacement [L]	1.12

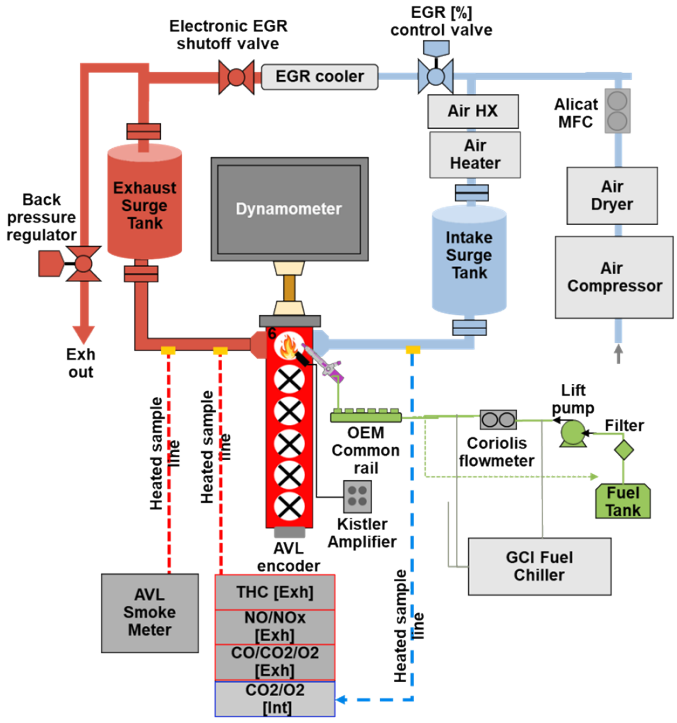

Figure 4. Modified 6.7 L diesel engine for single-cylinder operation configured for GCI operation with EGR with sampling port locations for exhaust and intake sampling identified.

The stock high-pressure common rail direct-injection (DI) fueling system and pump were used for the experiments. The fuel injector was the stock injector, which is a CRIN-3, eight-hole injector with a 145° included angle, and a nominal hole diameter of 140 µm. Fuel was supplied by a custom conditioning and measurement setup. The fuel conditioner contains a vapor eliminator along with regulators, internal heat exchangers, level controller, and a lift pump similar to what was used in work by Wissink et al. [19]. A Coriolis-effect mass flow meter from Micromotion was used to measure fuel flow rate. To help reduce cavitation and vapor, an external chiller was used to cool the engine supply fuel and the engine fuel return to 15°C, which is similar to previous experimental setups by Dempsey et al. [20]. Figure 5 shows a schematic of the DI combustion system highlighting the reentrant piston bowl shape and the spray targeting of the stock injectors.

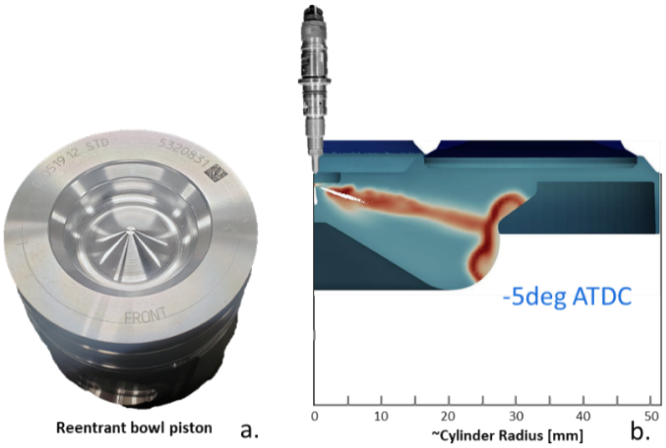

Figure 5. (a) Photograph of the stock reentrant bowl piston. (b) Illustration of direct-injected combustion system at −5° ATDC.

Compressed air for the intake charge was conditioned using a series of air dryers and particulate filters. The air temperature entering the engine was controlled using an automotive intercooler and a 6 kW air heater. Intake air mass flow rate was controlled through an Alicat mass flow controller (MFC). EGR and backpressure were controlled with electromechanical valves at the locations shown in Figure 4. Intake temperature was controlled downstream of where the fresh air and EGR were mixed. Given the highly pulsed nature of the single-cylinder exhaust, pulses were dampened through the use of 25 gal surge tanks on both the intake and exhaust, location as shown in Figure 4.

The engine coolant and oil temperature were maintained through an independent conditioning cart with heating and cooling capabilities. Oil circulation was provided by the stock internal engine oil pump, and coolant circulation was provided by an external ¾ horsepower single-phase circulation pump.

The engine was controlled using an open LabVIEW-based engine control system from NI Powertrain Controls (formerly Drivven), which provides full control authority over fuel injection timings and quantities for up to five injections per cycle as well as all other relevant parameters (e.g., rail pressure, airflow, EGR flow, and intake and exhaust manifold pressures). The system is capable of manual open-loop control of each actuator or closed-loop control for load, air-to-fuel ratio, EGR, manifold pressure, or other desired set points. For this study, manual setpoint control was used for all operating conditions.

High-speed in-cylinder pressure data were acquired using a Kistler model 6058A pressure transducer that was flush-mounted. A Kistler 5010 dual-mode amplifier was used. A custom, in-house LabVIEW-based Oak Ridge Combustion Analysis System (ORCAS) was used for data acquisition and real-time combustion analysis calculations. Cylinder pressure was pegged to the intake manifold pressure at bottom dead center of the intake stroke and sampled at a resolution of 0.2 crank angle degrees. Crank-angle resolved data, including cylinder pressure, were recorded for a minimum of 300 consecutive engine cycles at each operating condition.

Exhaust emissions were measured using a standard five-gas gaseous emissions bench with California Analytical Instrument analyzers via heated sample lines maintained at 190°C through heated filters with the housings, also maintained at 190°C. Parker type 100-25-DH21 filters composed of borosilicate glass microfibers were used to prevent soot and liquids from entering the emissions measurement system. Total NO_X ($NO + NO_2$) was measured using a heated chemiluminescence analyzer, CO and CO_2 were measured using nondispersive infrared analyzers, O_2 was measured using a paramagnetic analyzer, and total unburned hydrocarbon (HC) emissions were measured with a heated flame ionization detector. Separate O_2 and CO_2 measurements were made for the intake stream. Soot measurements were performed using an AVL 415S smoke meter, which uses a filter paper reflectance method to measure the black carbon containing soot in the exhaust as filter smoke number (FSN). For this study, the FSN was used to determine if low soot operation was successfully reached. Exhaust fuel-air equivalence ratio (ϕ) was calculated from the emissions bench and measured with an automotive wideband O_2 sensor in the exhaust.

2.2 Experimental Data Analysis

At each operating condition, ORCAS was used to calculate the apparent heat release rate (AHRR) and indicated work based on cylinder pressure data for each of the 300 consecutive cycles acquired. The AHRR is determined based on a first law of thermodynamics of the cylinder contents, estimating the ratio of specific heats using an average of the polytropic constants of compression and expansion determined by linear fits to the logarithms of pressure and volume. The AHRR was integrated to determine the mass fraction burned at each crank angle position, with start of combustion being determined by injection timing and end of combustion being the earlier of AHRR dropping below zero or exhaust valve opening. The values of AHRR, indicated work, and combustion phasing metrics for each cycle were then averaged over the 300 cycles in the data set during post-processing. Cylinder pressure and AHRR traces shown here are ensemble averages of the 300 acquired cycles.

Exhaust emissions calculations were performed using an open-source LabVIEW-based emissions calculator by Dempsey [20, 21], which was integrated into the ORCAS data acquisition system to determine ϕ, EGR fraction, and fuel-specific or indicated-work-specific emissions concentrations. EGR fractions were calculated on a mass basis after correcting the dry gas measurements of CO_2, CO, and O_2 for exhaust water concentration.

2.3 Fuels Investigated

The fuel used for this GCI study was US market-available gasoline with RON of 91 and AKI of 87, which contained no ethanol (E-0). Relevant properties are shown in Table 2. Similar to previous GCI studies conducted using a diesel fueling system [16, 19, 20, 22, 23], approximately 350 ppm of Infineum R655 lubricity additive was added to the 91 RON gasoline to protect the high-pressure common rail pump and DI injectors. The fuel analysis was performed with the 350 ppm of lubricity additive in the fuel at Southwest Research Institute using standard ASTM methods. For comparison purposes, a small number of CDC operating points was collected, and a 45 cetane number certification-grade ultra-low sulfur diesel fuel (ULSD) was used with relevant properties shown in

Table 3.

Table 2. Fuel properties for the gasoline fuel investigated.

Parameter	Value
RON [-]	91.0
MON [-]	83.3
Sensitivity (RON-MON)	7.7
AKI = (RON+MON)/2	87.1
Density	0.74
T10/T50/T90 [°C]	45/98/161
Aromatics vol %)]	30.4
Olefins [vol %)]	5.8
Saturates [vol %]	63.8
LHV [MJ/kg] via ASTM D240	43.436

Table 3. Fuel properties for the ULSD investigated

Parameter	Value
Cetane number [-] via ASTM D613	45.3
Density	0.849
T10/T50/T90 [°C]	205/260/308
Aromatics [vol %]	33.2
Olefins [vol %]	4.0
Saturates [vol %]	68.0
LHV [MJ/kg] via ASTM D240	42.631

2.4 Experimental Operating Conditions

The study used a constant engine speed of 1200 rpm and targeted a load of 4.3 bar IMEPg, which represents a low-load operating point for MD diesel engine applications. Fueling was adjusted to reach the target load with nominal injection conditions, and fuel quantity was held constant as injection timing and splits were swept, resulting in some variation in load around the nominal target. The LTC operational requirements for HFS and PFS GCI operating strategies, and control authority of combustion phasing via fuel injection parameters, were investigated in this study. The conditions for each of these operating points are outlined in the following subsections. Engine coolant and oil temperatures were kept constant at 95°C for all operating conditions. Self-imposed constraints for this study included a maximum pressure rise rate (MPRR) limit of 10 bar/degree and maximum HC emissions rate of 10,000 ppm.

2.4.1 HFS GCI Operation

For HFS operation, a split fuel injection strategy was used with a constant pilot advance of 10 CAD before the start of the main injection. This is a similar strategy used recently by Chuahy et al. [23]. Start of injection (SOI) sweeps were performed at 0%, 15%, 30%, and 50% EGR. The EGR sweep was performed with a constant intake manifold pressure and exhaust backpressure, such that intake airflow was reduced as EGR was increased. Intake air temperature was kept constant at 54°C, which is similar to other GCI studies [**Error! Bookmark not defined.**]. The fuel split between injection duration for pilot (Inj1) and main injection (Inj2) was kept constant across the sweep. Rail pressure was kept constant at 500 bar for all conditions. Previous research demonstrated that lower injection pressures can improve stratification compared with CDC-type rail pressures [3, 16, 20]. The operating conditions for HFS GCI operation are shown in Table 4.

Table 4. HFS operating conditions at a target load of 4.3 IMEPg.

Parameter	Value
Inj1-SOI/Inj2-SOI [°ATDC]	10° Adv./−1 to −12
Fuel in Inj1/Inj2 [ms]	0.71/ 0.31

Pin/Pexh	1.13/1.31
Intake temperature [°C]	54
EGR [%]	0, 15, 30, 50
Phi [-]	0.23–0.50
Rail pressure [bar]	500

2.4.2 PFS GCI Operation

For PFS operation, the target operating condition of 1,200 rpm, 4.3 bar IMEPg was found to have MPRR greater than the self-imposed study limit of 10 bar/degree for most operating variables considered. For the PFS operation at 1,200 rpm, 4.3 bar IMEPg, an injection strategy with an early injection at −260° ATDC (Inj1) with most of the fuel (~70%) was followed by a second injection (Inj2) with the remainder of the fuel. Results are presented in the next section for a second injection SOI sweep ranging from −40° to −3° ATDC at an EGR level of 15%; the operating conditions are shown in Table 5. This is a similar PFS strategy to that used in previous LD GCI investigations [**Error! Bookmark not defined.**, 23]. The intake pressure and exhaust backpressure, rail pressure, and intake temperature were matched to the 4.3 bar HFS case discussed in Section 2.4.1.

Table 5. PFS operating conditions at a target load of 4.3 bar IMEPg.

Parameter	Value
Target IMEPg [bar]	4.3
Inj1-SOI/Inj-2SOI [°ATDC]	−260/−40 to −3
Fuel in Inj1/Inj2 [ms]	0.71/0.31
Pin/Tin [bar/°C]	1.13/54
EGR [%]	15
Phi [-]	0.28
Rail pressure [bar]	500

To better understand the control authority that fuel energy split and injection timing had on control authority at low loads with this diesel engine configuration, additional studies were performed at 1,200 rpm, 3.0 bar IMEP. This load was chosen to avoid the self-imposed MPRR limit during the second injection SOI sweeps over the fuel energy split sweep with Inj2 quantity varying from 30% to approximately 70% of the fuel. The Inj1 timing was kept constant at the same −260° ATDC used in the 4.3 bar PFS operating strategy. These sweeps were performed at a 0% EGR level and a 40% EGR level. For the 0% EGR level, a naturally aspirated point was used. The intake temperature had to be raised to 63°C for stability. The operation conditions for the 1,200 rpm, 3.0 bar IMEPg PFS conditions are shown in Table 6.

Table 6: PFS Operating conditions for a target load of 3.0 bar IMEPg.

Operating condition	PFS fuel split sweep
Inj1-SOI/Inj2-SOI [°ATDC]	−260/−30
Fuel in Inj2 [ms]	0.31–0.71
EGR [%]/ Phi [-]	0/0.25, 40/0.33
Intake P ([kPa] /temperature [°C]	91/63 (0% EGR), 112/63 (40% EGR)

2.4.3 HFS with Diesel Fuel (CDC)

For a comparison of the control authority of CA50 and performance of HFS and PFS with market-grade gasoline against operation with diesel fuel, a CDC split injection strategy that mimicked the HFS injection strategy was used with an 8° constant advanced for Inj1. For the CDC operating points, boundary conditions were matched to that of the 4.3 bar IMEPg HFS operating point shown in Table 4. This does not represent any OEM injection strategy, but instead mirrors the GCI operating condition for a more direct comparison.

3 RESULTS AND DISCUSSION

The results of this study are presented in three subsections: the first subsection summarizes the HFS results at 1,200 rpm, 4.3 bar IMEPg; the second subsection presents PFS results at 1,200 rpm, 4.3 bar IMEPg and additional results at 3.0 bar IMEPg; the third subsection presents a comparison of selected HFS and PFS cases to CDC.

3.1 HFS Operation at 1,200 rpm, 4.3 bar IMEPg

Figure 6 shows the cylinder pressure and AHRR along with Inj2 (main injection) timing at the 0% EGR case to illustrate characteristics of HFS operation. Over this injection timing range, combustion phasing advanced with advancing Inj2 timing as expected with HFS. Figure 7 shows details of the AHRR traces. A change occurred over on the premixed spike as SOI advanced from −6° to −8° ATDC.

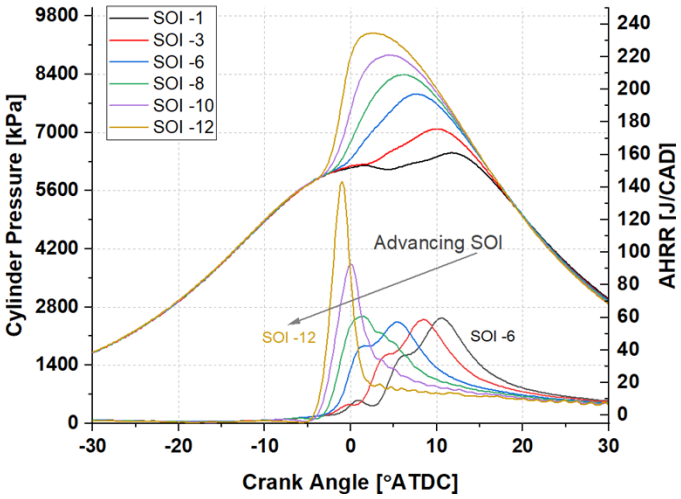

Figure 6. Cylinder pressure, AHRR, and Inj2 timing for the HFS nominal 4.3 bar IMEPg 0% EGR case.

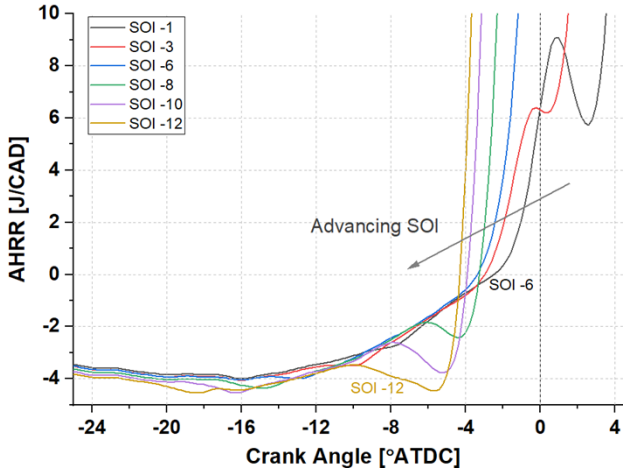

Figure 7. Details of AHRR and Inj2 timing for the HFS nominal 4.3 bar IMEPg 0% EGR case.

Figure 8Figure 8 shows the cylinder pressure and AHRR for the 15% and 50% EGR cases. Combustion phasing was retarded across all injection timings as EGR increased, but a similar level of control authority on CA50 occurred as a function of injection timing as was seen in the 0% EGR case.

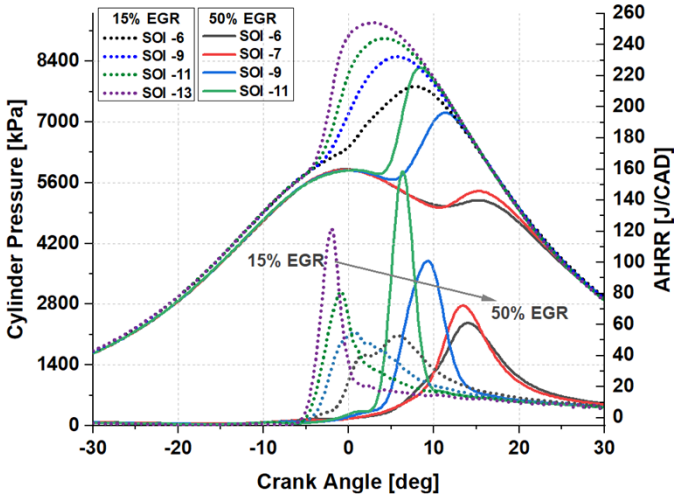

Figure 8. Cylinder pressure, AHRR, and Inj1 timing for the HFS nominal 4.3 bar IMEPg 15% EGR and 50% EGR cases.

Figure 9 details IMEPg, CA25, CA50, and MPRR across the injection timing sweeps across all of the EGR levels investigated for HFS with the target load of 4.3 bar IMEPg. IMEPg for the constant fueling sweeps fell at the most advanced combustion phasings for the 0%, 15%, and 30% EGR cases and dropped significantly for all but the most advanced phasings with the 50% EGR case. The limited SOI timings at 50% EGR result from the MPRR limit of 10 bar/degree at the most advanced injection timing and a HC limit of 10,000 ppm at the most retarded timing. A linear trend for CA25 was observed for all EGR cases; a significant retarding was seen for the 50% EGR case. A small effect on CA50 from the longer tail at the most advanced injection timings can be seen for the 15% and 30% EGR cases, with a more pronounced shift with the 50% EGR case as the phasings in general were greatly retarded. The direct link between combustion phasing and main SOI, which is characteristic of HFS operation, was still apparent even at these high EGR rates. MPRR also trended as expected with advancing CA50 with a sharp trend upward for the most advanced phasing. Additional discussion about the control authority of HFS is presented in Section 3.3.

Figure 10 shows emissions performance over the same injection timing sweep across all EGR levels. NO_X increased nonlinearly as combustion phasing was advanced and reduced with increasing EGR. The main SOI timing had a strong influence on NO_X emissions at the 0% and 15% cases, but this started to diminish at 30% and was minimal at 50% EGR. FSN trended in the opposite direction as NO_X, as was expected, and increased with retarded injection timings at the 30% EGR level. FSN was at or near the lower detection limit of the AVL 415S instrument across the entire injection timing sweep for the 50% EGR case. As EGR was increased, the main SOI had a stronger influence on CO and HC. ISHC values were low across the entire sweep but increased with retarding phasing and increasing EGR level. As combustion phasing was further retarded with the 50% EGR case, HC sharply increased, providing a narrow LTC injection timing band with low HC emissions with these reasonable boost pressures and intake temperatures. IMEPg and combustion efficiency were highest for the most advanced injection timings.

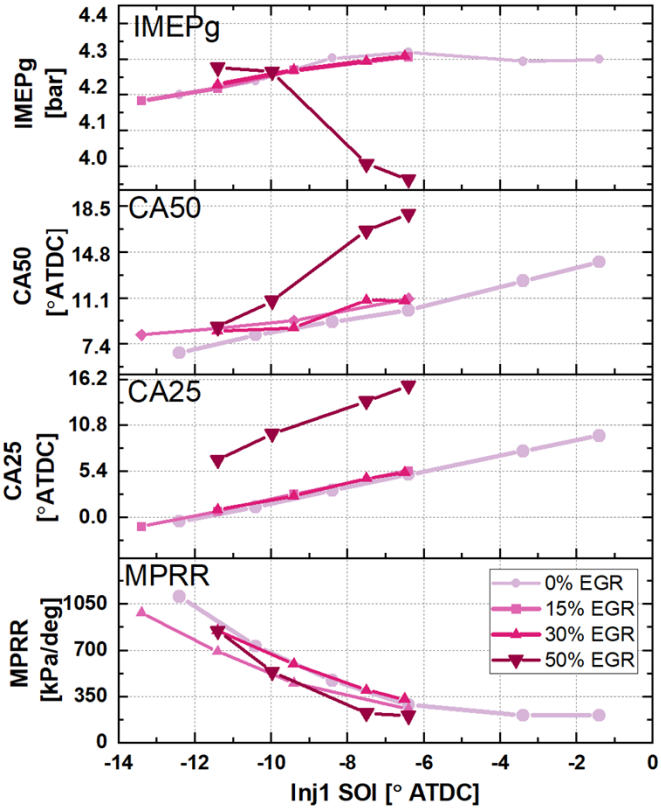

Figure 9. IMEPg, and combustion behavior of HFS at 1,200 rpm, 4.3 bar target IMEPg with 0% EGR as a function of Inj1 SOI.

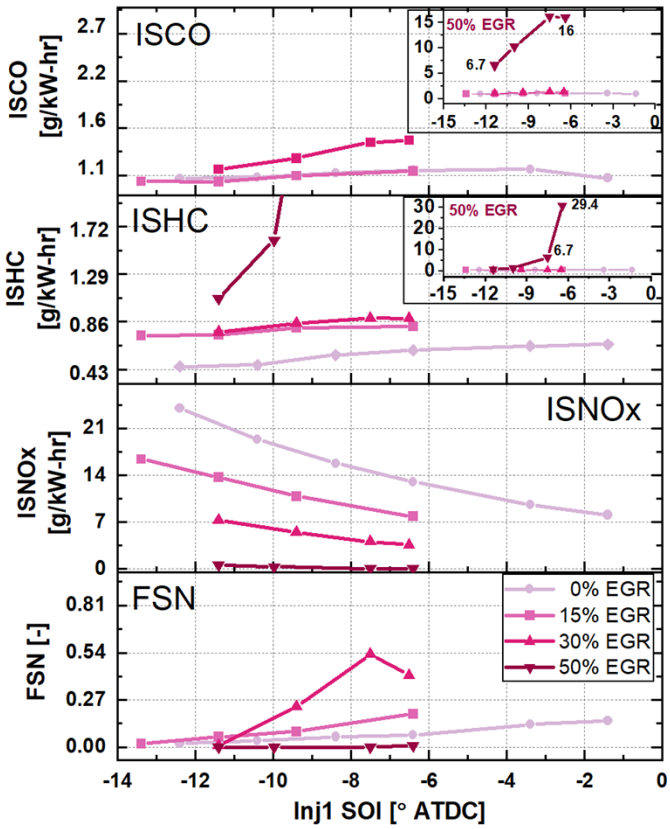

Figure 10. Emissions performance of HFS at 1,200 rpm, 4.3 bar target IMEPg at 0%, 15%, 30% and 50% EGR levels as a function of Inj1 SOI. (Inset of full-range ISCO and ISHC.)

Figure 11 shows a representative soot–NO_X trade-off over an EGR sweep from 0% to 50% across all the injection timings at each of the EGR levels studied. At the 50% EGR rate, intake O_2 concentration dropped to 16.3%. A constant CA50 line of ~9.0° ATDC illustrated the expected soot-NO_X trade-off. FSN values were low across most of the sweeps and were strongly influenced by injection timing. As has been seen in previous studies, an EGR rate of nearly 50% was needed to drive NO_X to very low levels.

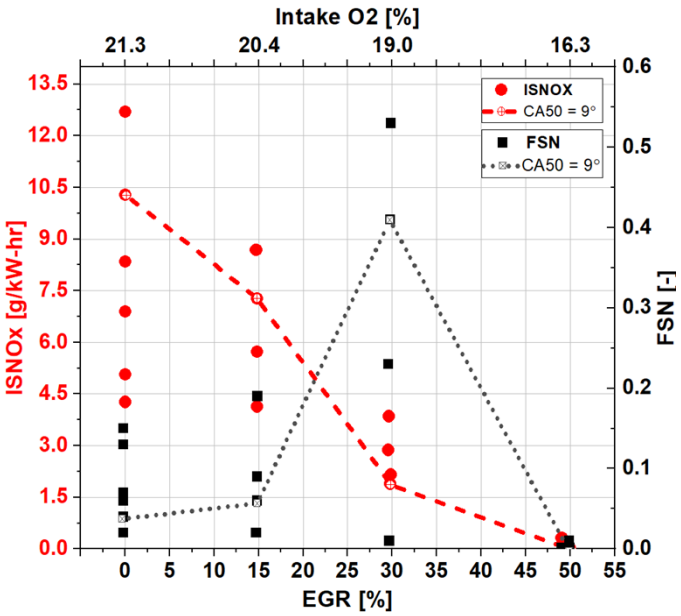

Figure 11. HFS FSN and NO_X as a function of increasing EGR level (with intake O_2 concentration on top *x*-axis) for all injection timing sweeps. NO_X and FSN for constant phasing of ~9° ATDC shown in dashed lines to emphasize NO_X/ FSN trade-off as a function of EGR/intake O_2.

3.2 PFS Operation at 1,200 rpm, 4.3 bar IMEPg, and 3.0 bar IMEPg

The following subsections present a summary of the PFS investigations performed. Section 3.2.1 summarizes the finding on a limited study of the effects of the Inj2 SOI sweep at 1,200 rpm, 4.3 bar IMEPg with an EGR rate of 15% with matched intake pressure, exhaust backpressure, and intake temperature as the HFS operating conditions. As discussed in Section 2.4.2, the 4.3 bar PFS operating point was at or near the self-imposed 10 bar/degree MPRR limit for this study. Section 3.2.2 presents a detailed investigation of Inj2 timing sweeps and Inj1/Inj2 fuel quantity at a lower load of 1,200 rpm, 3.0 bar IMEPg at 0% and 40% EGR.

3.2.1 PFS Operation 4.3 bar IMEPg

Figure 12 shows in-cylinder pressure and AHRR for the Inj2 timing sweep from −40° ATDC to −3° TDC with a fixed Inj1 timing of −260° ATDC. Figure 13 shows a close-up of the AHRR. Similar to what has been observed in other PFS studies with lower intake pressures, there was little change in combustion phasing as measured by the crank angle at which 50% of the fuel energy was released (CA50), combustion efficiency, or MPRR from a Inj2 SOI of −40° ADTC to −20° ADTC. Performance was generally flat across the SOI sweep. A shift in combustion phasing occurred at a Inj2 SOI of −15° ATDC. Figure 13Figure 13 shows a notable difference where a small, premixed spike in the AHRR with the latest Inj2 SOIs was not observed in the earlier injection timings.

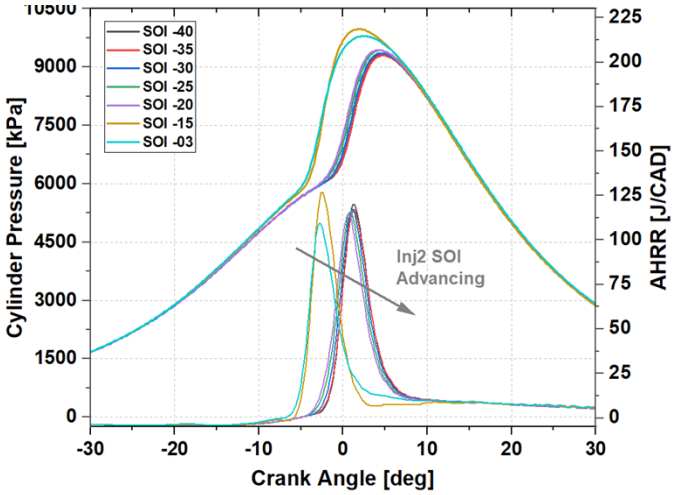

Figure 12. Cylinder pressure, AHRR, and Inj2 timings over SOI sweep with fixed Inj1 SOI at −260 ATDC for PFS operation at 1,200 rpm, 4.3 bar IMEPg with 15% EGR.

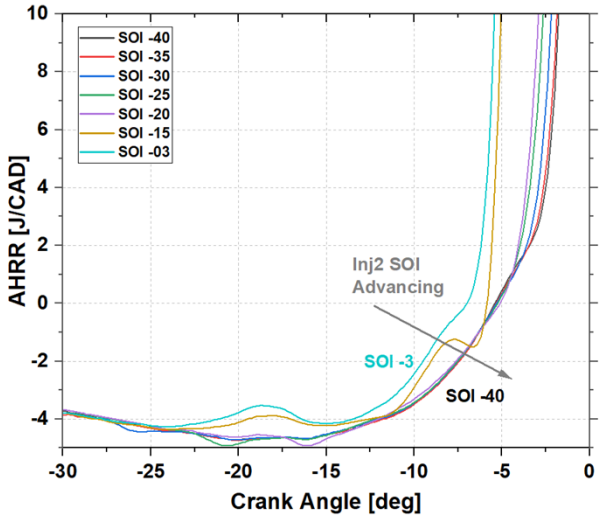

Figure 13. Close-up of AHRR for PFS Inj2 SOI sweep with fixed Inj1 SOI at −260° ATDC for PFS operation at 1,200 rpm, 4.3 bar IMEPg with 15% EGR.

Combustion duration spread out slightly for the −3° Inj2 SOI as compared with the −15° Inj2 SOI case as seen by similar CA25 but later CA50 with the SOI −3° case as shown in Figure 14. Further investigation using computational fluid dynamics will be needed to determine the nature of the shift in performance and what role fuel/piston interactions have with this experimental setup.

This shift in combustion phasing at the Inj2 SOI approached TDC results in a significant increase in NO_X and decrease in HC as shown in Figure 15 with this effect seen at the more retarded INj2 SOIs. This transition point was also observed by the sudden change in MPRR. During the majority of the SOI sweep, engine-out NO_X was measured at the 1–3 ppm range (0.11–0.13 g/kW-hr [0.066–0.077 g/kg-fuel]) with elevated HC (~7 g/kW-hr [43 g/kg-fuel]) and near-zero FSN (<0.05) as shown in Figure 15. These findings for the ability of PFS to achieve very low NO_X and soot as measured by FSN and elevated HC are characteristic of PFS operation, but with reduced control authority over combustion phasing at low boost levels.

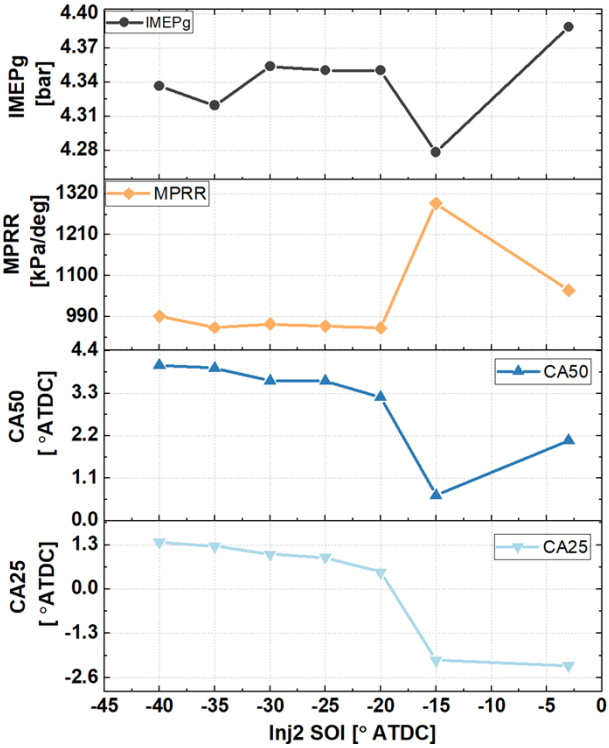

Figure 14. Performance of PFS at 1,200 rpm, 4.3 bar IMEPg with 15% EGR over a Inj2 timing sweep.

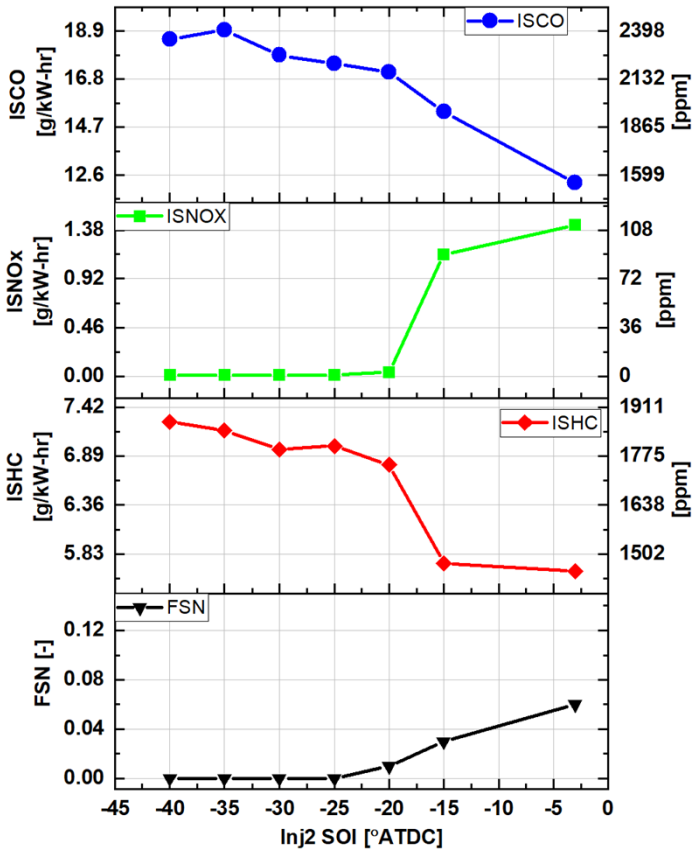

Figure 15. Emissions and efficiency performance for PFS operation at 1,200 rpm, 4.3 bar IMEPg with 15% EGR. Concentration values from CO, NO_X, and HC shown on the right *y*-axis.

3.2.2 PFS Operation 3.0 bar IMEPg

To further investigate the role of fuel injection quantity split and Inj2 SOI timing, additional experiments were conducted at lower load of 1,200 rpm, 3.0 bar IMEPg to avoid exceeding the MPRR limit discussed previously. Although all the results show similar behavior, a selected case of 0% EGR with a main SOI of −30° ATDC is presented for discussion. The Inj1 timing was maintained at −260° ATDC, and the injection duration was varied from 0.71 to 0.31 ms in Inj1 with load balanced by increasing duration in Inj2. Figure 16 shows the cylinder pressure and AHRR as the fuel split was adjusted at a representative case with Inj2 timing of −30° ATDC. Details of heat release up through TDC in Figure 16 show what is expected to be an evaporative cooling affect from the injected fuel that advanced as the duration of Inj2 increases. Figure 17 shows the 40% EGR case with Inj2 SOI of −30° ATDC.

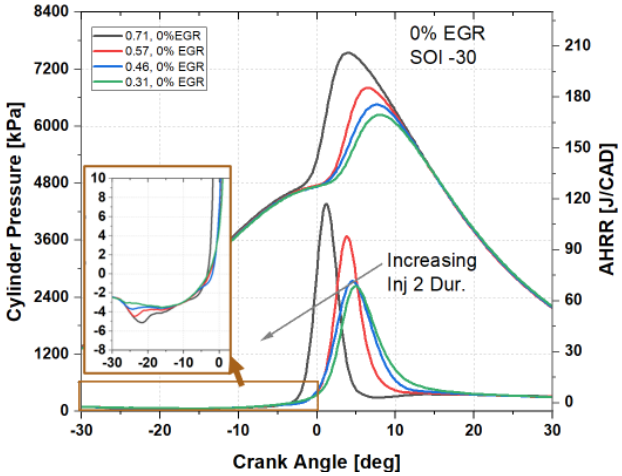

Figure 16. Cylinder pressure and AHRR for 3.0 bar IMEPg PFS fuel split sweep at Inj2 SOI of 30° ATDC with 0% EGR. Inset shows AHRR from −30° to ~0° ATDC.

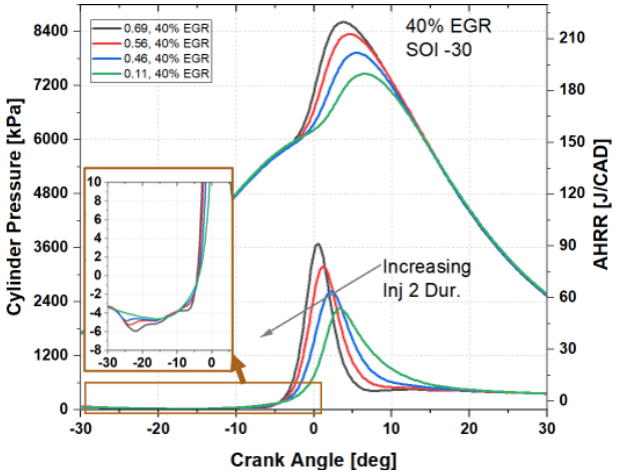

Figure 17. Cylinder pressure and AHRR for 3.0 bar IMEPg PFS fuel split sweep at Inj2 SOI of 30° ATDC with 40% EGR. Inset shows AHRR from −30° to ~0° ATDC.

Figure 18 shows the performance over the 1,200 rpm, 3.0 bar IMPEg target PFS fuel split sweeps with the Inj2 timing of −30° ATDC for both EGR levels. Despite the large change in the ratio between the fuel quantity in Inj1 and Inj2, only minor differences in combustion phasing were observed. The load was relatively flat across the sweep with a small increase observed at the most advanced phasing, which corresponds to a sharp increase in NO_X and a significant reduction in HC emissions as shown in Figure 19. It is not until the duration of Inj2 reached 0.71 ms that there was a significant difference in NO_X or HC emissions with the 0% EGR case. The results were mostly similar for the 40% EGR case, but the higher EGR fraction suppressed the NO_X increase at the highest Inj2 duration observed with the 0% EGR case.

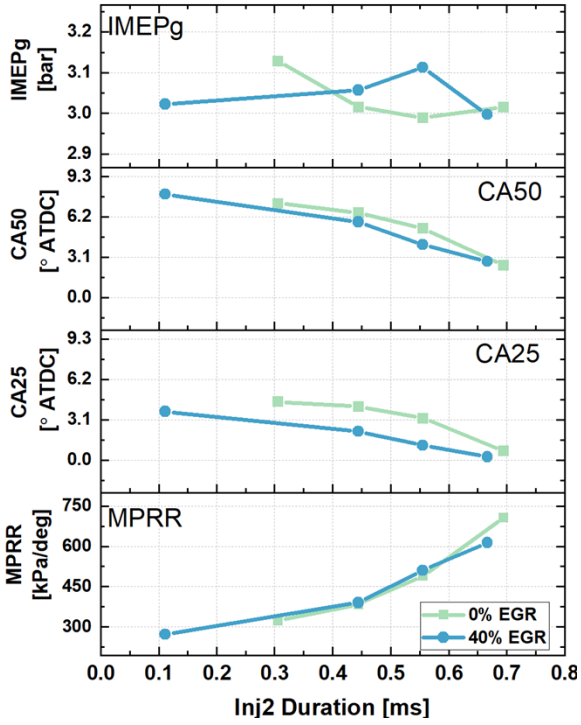

Figure 18. IMEP, CA50, CA25 and MPRR for 1,200 rpm, 3.0 bar IMEPg PFS fuel split at a Inj2 SOI of 30° ATDC with 0% EGR.

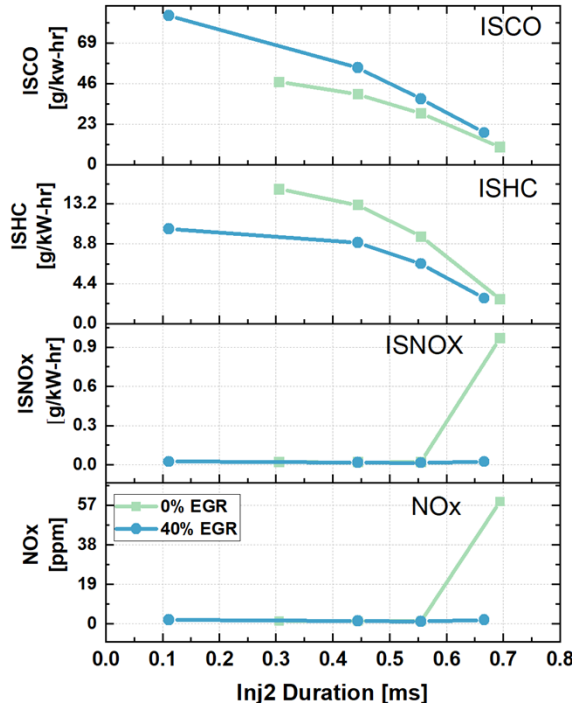

Figure 19. Emissions comparison of 0% and 40% EGR cases for the 1,200 rpm, 3.0 bar IMEPg PFS with Inj2 SOI of 30° ATDC.

3.2.3 Diesel combustion at 1,200 rpm 4.3 bar IMEPg

Figure 20 shows the cylinder pressure and AHRR as a function of main injection timing for a 1,200 rpm, 4.3 bar IMEPg target CDC with certification ULSD. This case used a similar injection strategy as the HFS cases but with an 8°advance for Inj1. In addition, boundary conditions to the HFS cases were matched to illustrate the differences in operation due to the use of diesel fuel compared with gasoline. The details of the control authority and emissions performance are not detailed in this section but are instead used for broader comparisons to HFS and PFS in the next section.

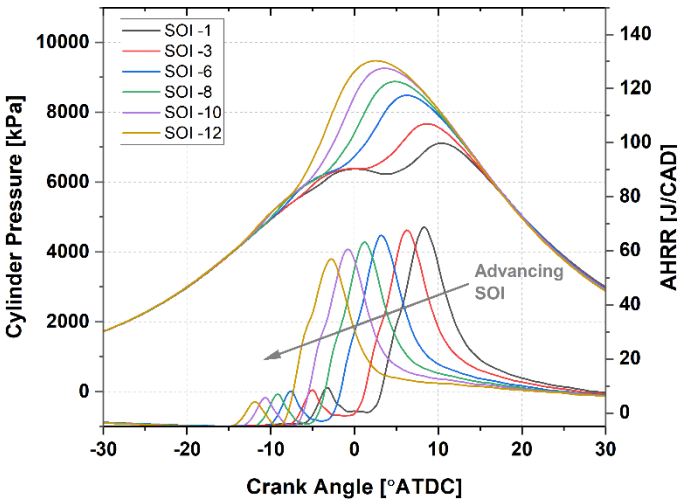

Figure 20. 1,200 rpm, 4.3 bar IMEP CDC injection timing sweep for 0% EGR with injection schedule and boundary conditions matched to the 0% EGR HFS case.

3.3 Comparison of HFS and PFS to CDC

3.3.1 Control Authority of Combustion Phasing via Injection Timing

The control authority over combustion phasing with main injection SOI was investigated during the sweeps of EGR and main SOI timing presented in Section 3.1. HFS is characterized by a strong controllability of combustion phasing with main SOI. Figure 21 shows the control authority over both CA25 and CA50 as a function of Inj2 SOI for HFS with both 0% and 15% EGR levels, the PFS case at 15% EGR, and a 0% EGR CDC case using a 45-cetane diesel fuel, all at a target load of 4.3 IMEPg. The HFS results show nearly the same level of control authority as the CDC case with some offset due to increased ignition delay with the 87 AKI gasoline. The results for the other EGR rates have a similar control authority as a function of main SOI timing. In contrast to the HFS operation, the PFS operation showed relatively little combustion phasing control over a much wider range of SOI timings. For the Inj2 SOI sweep from −40 to −3° ATDC at the target load of 4.3 bar IMEPg, the total change in CA50 combustion phasing was less than 4°. As mentioned in the previous section, for the fuel split investigations at 3.0 bar IMEPg, a 3° change in CA50 was seen over the sweep of main duration changing from 0.31 to 0.71 ms. These results are similar to the level of control authority seen in previous GCI investigations with a range of RON for gasoline–boiling range fuel on a multi-cylinder LD diesel engine mentioned in Section 1 [**Error! Bookmark not defined.**].

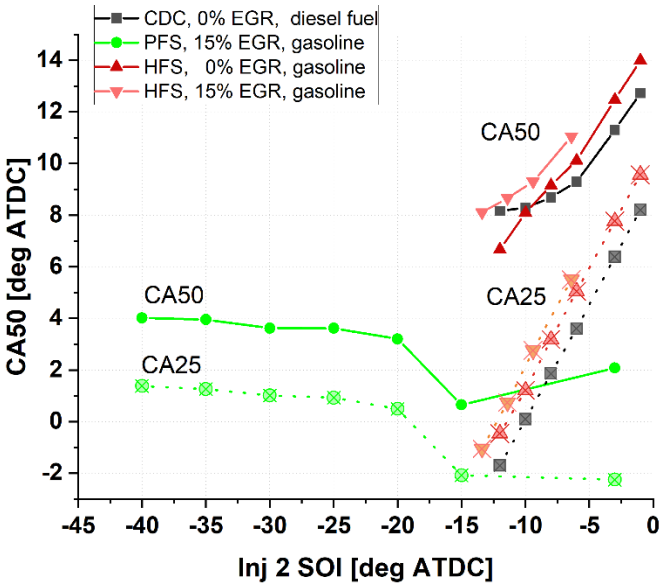

Figure 21. Location of CA25 (dashed) and CA50 (solid) as a function of main SOI timing (Inj2) for 1,200 rpm, 4.3 bar IMEP for CDC with 0% EGR using diesel fuel, HFS at 0% EGR and 15% EGR levels, and PFS at 15% EGR.

3.3.2 Comparison of Performance

A comparison of selected low-load GCI operation against a similar operating point with CDC is shown below to highlight some key benefits and challenges. Table 7 shows the operating parameters of the comparison points all at 1,200 rpm, 4.3 bar IMEPg with matched intake pressure and exhaust backpressure. Two CDC cases are presented: a 0% EGR case with a main SOI of −6.1 ATDC and a 50% EGR case with a main SOI of −6.1 ATDC. As mentioned previously, the CDC operating strategy does not mimic any OEM strategy and used a pilot advance of 8° to have commonality with the GCI operating points. The GCI operating points include a representative LTC PFS case with a Inj2 at −30° ATDC with an EGR rate of 15%. Two HFS cases are presented: a LTC HFS case with a 50% EGR rate with a main SOI of 9.4° ATDC and a non-LTC MCCI HFS case with a 15% EGR level with a main SOI of −6.4° ATDC.

Table 7. Operating conditions across different combustion modes with gasoline and ULSD at 1,200 rpm, 4.3 bar IMEPg.

Parameter	CDC 0% EGR	CDC 50% EGR	HFS 0% EGR	HFS 50% EGR	HFS 50% EGR	PFS LTC
Fuel	ULSD	ULSD	Gas.	Gas.	Gas.	Gas.
Inj1 [ATDC]	−14.1	−14.1	−18.4	−17.5	−19.95	−260
Inj 2 [ATDC]	−6.1	−6.1	−8.4	−7.5	−9.9	−30
Rail P [bar]	750	750	500	500	500	500
EGR [%]	0	50	0	50	50	15

Figure 22 compares ITEnet, NO_X, HC, exhaust port temperature, MPRR and CA50, for the selected operating cases. The HFS and PFS cases had slightly improved efficiency compared with the CDC cases with 15% and 50% EGR. Efficiency error bars shown represent the upper and lower bounds of measured fuel flow. PFS showed superior NO_X performance with NO_X near the detection limit of the HCLD,

although with increased HC emissions. HFS operation showed a marked reduction in FSN for both the LTC and MCCI cases compared with CDC. HFS showed low HC emission and ability to achieve LTC with high EGR rates. The sensitivity for the high EGR HFS cases to combustion phasing and NO_X/HC was apparent with the two cases shown below in which very low NO_X was possible but quickly approached a strong trade-off with late combustion phasings. For similar phasings, HFS and CDC both had a high ITE with NO_X being lower for CDC, and HC being higher for HFS.

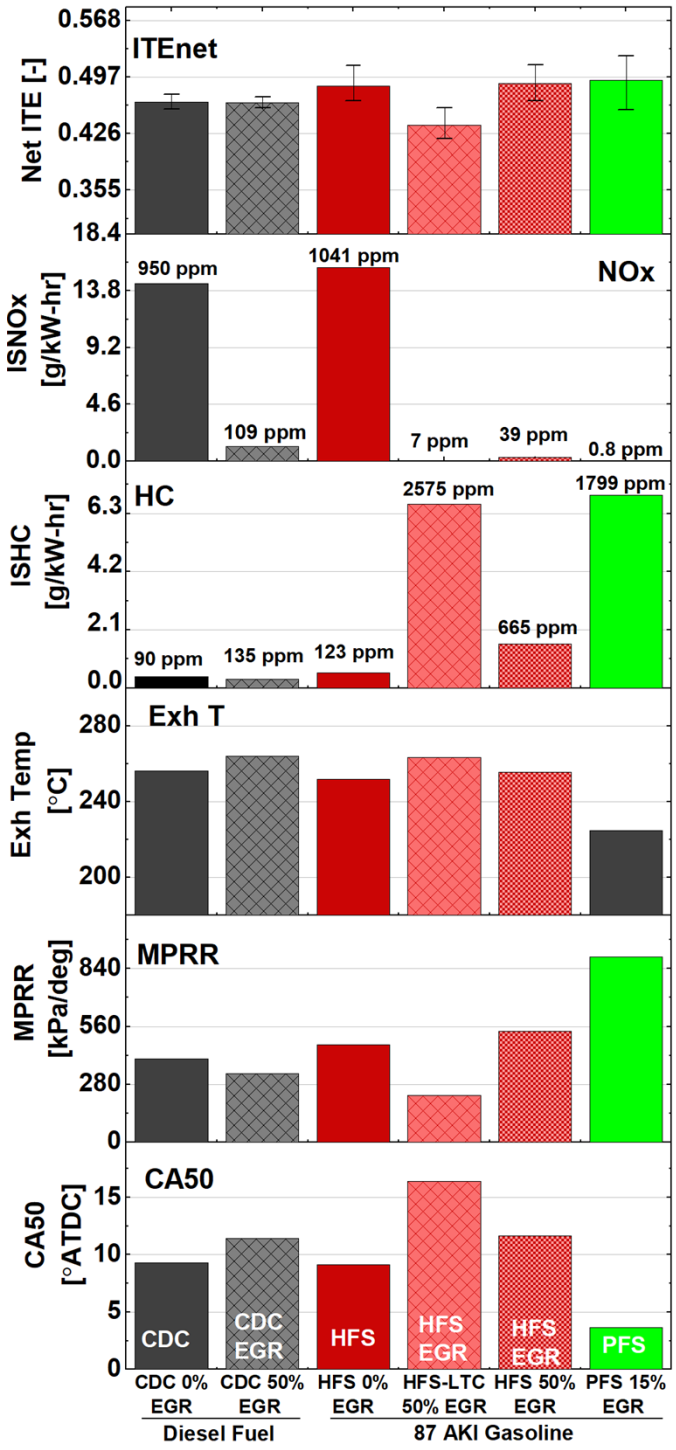

Figure 22 Efficiency, emissions, and CA50 for CDC at 0% and 50% EGR, HFS at 0% and 505 EGR, and PFS at 15% EGR at 1,200 rpm, 4.3 bar IMEP. ITEnet bars show ITEnet with minimum and maximum fuel flow measured.

4 Conclusions

In this work, a MD single-cylinder engine was used to investigate the low-load performance of GCI using a market-available 87 AKI gasoline with a focus on achieving LTC at the two ends of the fuel-air stratification spectrum. Both HFS and PFS operation indicated thermal efficiencies at or above mixing controlled operation with diesel fuel. Successful translation of conceptual approach of fuel injection timing and stratification levels for GCI operation to MD platform, including the ability to run in LTC or non-LTC GCI modes with efficiencies at or above those achieved with similar injection strategies with diesel fuel, was shown. The ability to use market-grade gasoline for GCI operation with stock diesel hardware without additional optimization to the injector or combustion chamber at lower loads was also shown. The high surface to volume ratio, greater distances between injector and wetted surfaces, and low swirl all are well suited for GCI.

- HFS operation at 1,200 rpm, 4.3 IMEPg showed high control authority of combustion phasing as a function of injection timing and an EGR requirement of approximately 50% to achieve very low NO_X and soot. The 87 AKI gasoline provided benefits in terms of volatility, and ignition delay provided a significant soot benefit compared with a similar operating strategy with diesel fuel as expected.
- PFS operation showed very low NO_X and soot in LTC modes with no significant EGR requirements but had little control authority over combustion phasing or duration with injection timing. The maximum load with the higher compression ratio of this engine platform was reduced from previous/similar work [16]. In the LD engine study, this narrow range of CA50 authority was insufficient to control the inherent cylinder-to-cylinder differences that occur in multi-cylinder engines.

Questions that remain include how to optimize system performance with emissions control systems, and whether HC or NO_X will be more costly and difficult to control over a drive cycle. Additional questions on how best to use multiple injection strategies over an entire engine map and what speed and load effects will control authority also remain. Further investigation using computational fluid dynamics will be needed to determine the nature of the shift in performance and what role fuel/piston interactions have with this experimental setup, which could lead to further optimization of the injector and piston bowl for further increases in efficiency and reduction in HC and CO emissions.

References

1. Reitz, R. D., Ogawa, H., Payri, R., et al. IJER editorial: The future of the internal combustion engine. Journalism 21(1): 327–344, 2020. doi:10.1177/1464884919862655
2. Davis, S., and Boundy, R., Transportation energy data book: edition 39. 2020. https://tedb.ornl.gov/wp-content/uploads/2021/02/TEDB_Ed_39.pdf
3. Lerin, C., Edwards, K. D., Curran, S. J., et al. Exploring the potential benefits of high-efficiency dual-fuel combustion on a heavy-duty multi-cylinder engine for SuperTruck I. International Journal of Engine Research. 2021. doi: 10.1177/14680874211006943
4. Dempsey, A., Curran, S., and Wagner, R., A perspective on the range of gasoline compression ignition combustion strategies for

high engine efficiency and low NO_X and soot emissions: Effects of in-cylinder fuel stratification. International Journal of Engine Research 17(8), 897–917, 2016, doi: 10.1177/1468087415621805
5. Dec, J., Dernotte, J., and Ji, C., "Increasing the Load Range, Load-to-Boost Ratio, and Efficiency of Low-Temperature Gasoline Combustion (LTGC) Engines," SAE Int. J. Engines 10(3):2017, doi:10.4271/2017-01-0731.
6. Zhang, Y, Kumar, P, Tang, M, Pei, Y, Merritt, B, Traver, M, & Popuri, S. "Impact of Geometric Compression Ratio and Variable Valve Actuation on Gasoline Compression Ignition in a Heavy-Duty Diesel Engine." Proceedings of the ASME 2020 Internal Combustion Engine Division Fall Technical Conference. ASME 2020 Internal Combustion Engine Division Fall Technical Conference. Virtual, Online. November 4–6, 2020. V001T03A016. ASME. https://doi.org/10.1115/ICEF2020-3035
7. Zhao, L, Pei, Y, Zhang, Y, Kumar, P, Tzanetakis, T, Traver, M, & Ameen, M. "Numerical Evaluation of Spray-Guided Glow Plug Assistance on Gasoline Compression Ignition During Cold Idle Operation in a Heavy-Duty Diesel Engine." Proceedings of the ASME 2020 Internal Combustion Engine Division Fall Technical Conference. ASME 2020 Internal Combustion Engine Division Fall Technical Conference. Virtual, Online. November 4–6, 2020. V001T06A010. ASME.
8. Tang, M, Pei, Y, Guo, H, Zhang, Y, Torelli, R, Probst, D, Fütterer, C, & Traver, M. "Piston Bowl Geometry Effects on Gasoline Compression Ignition in a Heavy-Duty Diesel Engine." Proceedings of the ASME 2020 Internal Combustion Engine Division Fall Technical Conference. ASME 2020 Internal Combustion Engine Division Fall Technical Conference. Virtual, Online. November 4–6, 2020. V001T06A011. ASME. https://doi.org/10.1115/ICEF2020-2990
9. Dec, J., Yang, Y., Dernotte, J., and Ji, C., "Effects of Gasoline Reactivity and Ethanol Content on Boosted, Premixed and Partially Stratified Low-Temperature Gasoline Combustion (LTGC)," SAE Int. J. Engines 8(3):2015, doi:10.4271/2015-01-0813.
10. Lopez Pintor, D., Gentz, G., and Dec, J., "Mixture Stratification for CA50 Control of LTGC Engines with Reactivity-Enhanced and Non-Additized Gasoline," SAE Technical Paper 2021-01-0513, 2021, doi:10.4271/2021-01-0513.
11. Roberts, J., Chuahy, F., Kokjohn, S., and Roy, S., "Isolation of the parametric effects of pre-blended fuel on low load gasoline compression ignition (GCI)", Fuel, Volume 237, 2019, Pages 522-535, ISSN 0016-2361, https://doi.org/10.1016/j.fuel.2018.09.150.
12. Babu, A., Roberts, J., and Kokjohn, S., "Effects of Fuel Properties and Composition on Low-Load Gasoline Compression Ignition Strategies," SAE Int. J. Engines 14(2):151-171, 2021, https://doi.org/10.4271/03-14-02-0010.
13. Cung, K., Bitsis, D.C., Miwa, J., Smith, E. et al., "Investigation of Gasoline Compression Ignition (GCI) Combustion in a High Compression-Ratio Heavy-duty Single-Cylinder Diesel Engine," SAE Technical Paper 2021-01-0495, 2021, doi:10.4271/2021-01-0495.
14. Hildingsson, L., Johansson, B., Kalghatgi, G., and Harrison, A., "Some Effects of Fuel Autoignition Quality and Volatility in Premixed Compression Ignition Engines," SAE Int. J. Engines 3(1):440-460, 2010, https://doi.org/10.4271/2010-01-0607.
15. Manente, V., Johansson, B., Tunestal, P., and Cannella, W., "Effects of Different Type of Gasoline Fuels on Heavy Duty Partially Premixed Combustion," SAE Int. J. Engines 2(2):71-88, 2010, https://doi.org/10.4271/2009-01-2668.
16. Dempsey, AB, Curran, S, Wagner, R, Cannella, W, & Ickes, A. "Gasoline Compression Ignition (GCI) on a Light-Duty Multi-Cylinder Engine Using a Wide Range of Fuel Reactivities and Heavy Fuel Stratification." Proceedings of the ASME 2020 Internal Combustion Engine Division Fall Technical Conference. ASME 2020 Internal Combustion Engine Division Fall Technical Conference. Virtual, Online. November 4–6, 2020. V001T03A004. ASME. https://doi.org/10.1115/ICEF2020-2929
17. "Fuel/Engine Interactions" Kalghatgi, G., 2014 SAE International, Warrendale, Pa, ISBN 878-0-7680-6458-2
18. ASTM D4814-21, Standard Specification for Automotive Spark-Ignition Engine Fuel, Jan 12, 2021.
19. Wissink ML, Curran SJ, Roberts G, Musculus MP, Mounaïm-Rousselle C. Isolating the effects of reactivity stratification in reactivity-controlled compression ignition with iso-octane and n-heptane on a light-duty multi-cylinder engine. International Journal of Engine Research. 2018;19(9):907-926. doi:10.1177/1468087417732898
20. Dempsey, A, Curran, S, Wagner, R, & Cannella, W. "Effect of Premixed Fuel Preparation for Partially Premixed Combustion With a Low Octane Gasoline on a Light-Duty Multi-Cylinder Compression Ignition Engine." Proceedings of the ASME 2014 Internal Combustion Engine Division Fall Technical Conference. Volume 1: Large Bore Engines; Fuels; Advanced Combustion; Emissions Control Systems. Columbus, Indiana, USA. October 19–22, 2014. V001T03A012. ASME. https://doi.org/10.1115/ICEF2014-5561
21. Engine Emissions & Uncertainty Analysis, Dempsey, A., https://sourceforge.net/projects/engine-emissions-uncertainty/files/ [software] 2016
22. Moses-DeBusk, M., Curran, S.J., Lewis, S.A. et al. Impacts of Air-Fuel Stratification in ACI Combustion on Particulate Matter and Gaseous Emissions. Emiss. Control Sci. Technol. 5, 225–237 (2019). https://doi.org/10.1007/s40825-019-00122-5
23. Chuahy, F., DeBusk., M., Curran, S., Storey, J., "The effects of distillation characteristics and aromatic content on low-load gasoline compression ignition (GCI) performance and soot emissions in a multi-cylinder engine" Fuel, 2021,

Contact Information

Scott Curran, CurranSJ@ornl.gov

Acknowledgments

This research was supported by the Department of Energy's (DOE's) Office of Energy Efficiency and Renewable Energy (EERE), Vehicle Technologies Office and used resources at the National Transportation Research Center, a DOE-EERE User Facility at Oak Ridge National Laboratory. The authors would gratefully like to thank the U.S. DOE Vehicle Technologies Office Program Managers Michael Weismiller and Gurpreet Singh for the support and guidance for this work. The authors would like to thank the generous support from Cummins, including Tim Lutz and many others, for supplying the engine used for this study and providing support for the machining of the cylinder head for flush mount pressure transducers. The authors would also like to thank Infinium for supplying the R655 lubricity additive used in this study. Special thanks to Steve Whitted, Scott Palko, Martin Wissink, and Chloe Lerin at Oak Ridge National Laboratory for supporting the design and build of the single-cylinder engine setup used for this study and to Flavio Chuahy for generating the graphic used in Figure 5.

Appendix

The Appendix is one-column. If you have an appendix in your document, you will need to insert a continuous page break and set the columns to one. If you do not have an appendix in your document, this paragraph can be ignored and the heading and section break deleted.

---

1 Reitz RD, Ogawa H, Payri R, et al. IJER editorial: The future of the internal combustion engine. Journalism. 2020;21(1):327-344. doi:10.1177/1464884919862655

2 Davis, S and Boundy, R., Transportation energy data book: edition 39—2020, https://tedb.ornl.gov/wp-content/uploads/2021/02/TEDB_Ed_39.pdf

3. A. B. Dempsey, S. J. Curran, and R. M. Wagner, "A perspective on the range of gasoline compression ignition combustion strategies for high engine efficiency and low NOx and soot emissions: Effects of in-cylinder fuel stratification," *Int. J. Engine Res.*, vol. 17, no. 8, 2016, doi: 10.1177/1468087415621805

4 Paz, J., Staaden, D., and Kokjohn, S., "Gasoline Compression Ignition Operation of a Heavy-Duty Engine at High Load," SAE Technical Paper 2018-01-0898, 2018, doi:10.4271/2018-01-0898.

5 Dec, J., Dernotte, J., and Ji, C., "Increasing the Load Range, Load-to-Boost Ratio, and Efficiency of Low-Temperature Gasoline Combustion (LTGC) Engines," SAE Int. J. Engines 10(3):2017, doi:10.4271/2017-01-0731.

6 Zhang, Y, Kumar, P, Tang, M, Pei, Y, Merritt, B, Traver, M, & Popuri, S. "Impact of Geometric Compression Ratio and Variable Valve Actuation on Gasoline Compression Ignition in a Heavy-Duty Diesel Engine." Proceedings of the ASME 2020 Internal Combustion Engine Division Fall Technical Conference. ASME 2020 Internal Combustion Engine Division Fall Technical Conference. Virtual, Online. November 4–6, 2020. V001T03A016. ASME. https://doi.org/10.1115/ICEF2020-3035

7 Zhao, L, Pei, Y, Zhang, Y, Kumar, P, Tzanetakis, T, Traver, M, & Ameen, M. "Numerical Evaluation of Spray-Guided Glow Plug Assistance on Gasoline Compression Ignition During Cold Idle Operation in a Heavy-Duty Diesel Engine." Proceedings of the ASME 2020 Internal Combustion Engine Division Fall Technical Conference. ASME 2020 Internal Combustion Engine Division Fall Technical Conference. Virtual, Online. November 4–6, 2020. V001T06A010. ASME.

8 Tang, M, Pei, Y, Guo, H, Zhang, Y, Torelli, R, Probst, D, Fütterer, C, & Traver, M. "Piston Bowl Geometry Effects on Gasoline Compression Ignition in a Heavy-Duty Diesel Engine." Proceedings of the ASME 2020 Internal Combustion Engine Division Fall Technical Conference. ASME 2020 Internal Combustion Engine Division Fall Technical Conference. Virtual, Online. November 4–6, 2020. V001T06A011. ASME. https://doi.org/10.1115/ICEF2020-2990

9 Dec, J., Yang, Y., Dernotte, J., and Ji, C., "Effects of Gasoline Reactivity and Ethanol Content on Boosted, Premixed and Partially Stratified Low-Temperature Gasoline Combustion (LTGC)," SAE Int. J. Engines 8(3):2015, doi:10.4271/2015-01-0813.

10 Lopez Pintor, D., Gentz, G., and Dec, J., "Mixture Stratification for CA50 Control of LTGC Engines with Reactivity-Enhanced and Non-Additized Gasoline," SAE Technical Paper 2021-01-0513, 2021, doi:10.4271/2021-01-0513.

11 Roberts, J., Chuahy, F., Kokjohn, S., and Roy, S., "Isolation of the parametric effects of pre-blended fuel on low load gasoline compression ignition (GCI)", Fuel, Volume 237, 2019, Pages 522-535, ISSN 0016-2361, https://doi.org/10.1016/j.fuel.2018.09.150.

12. Babu, A., Roberts, J., and Kokjohn, S., "Effects of Fuel Properties and Composition on Low-Load Gasoline Compression Ignition Strategies," SAE Int. J. Engines 14(2):151-171, 2021, https://doi.org/10.4271/03-14-02-0010.

13 Cung, K., Bitsis, D.C., Miwa, J., Smith, E. et al., "Investigation of Gasoline Compression Ignition (GCI) Combustion in a High Compression-Ratio Heavy-duty Single-Cylinder Diesel Engine," SAE Technical Paper 2021-01-0495, 2021, doi:10.4271/2021-01-0495.

14. Hildingsson, L., Johansson, B., Kalghatgi, G., and Harrison, A., "Some Effects of Fuel Autoignition Quality and Volatility in Premixed Compression Ignition Engines," SAE Int. J. Engines 3(1):440-460, 2010, https://doi.org/10.4271/2010-01-0607.

15. Manente, V., Johansson, B., Tunestal, P., and Cannella, W., "Effects of Different Type of Gasoline Fuels on Heavy Duty Partially Premixed Combustion," SAE Int. J. Engines 2(2):71-88, 2010, https://doi.org/10.4271/2009-01-2668.

16. Dempsey, AB, Curran, S, Wagner, R, Cannella, W, & Ickes, A. "Gasoline Compression Ignition (GCI) on a Light-Duty Multi-Cylinder Engine Using a Wide Range of Fuel Reactivities and Heavy Fuel Stratification." Proceedings of the ASME 2020 Internal Combustion Engine Division Fall Technical Conference. ASME 2020 Internal Combustion Engine Division Fall Technical Conference. Virtual, Online. November 4–6, 2020. V001T03A004. ASME. https://doi.org/10.1115/ICEF2020-2929

17. "Fuel/Engine Interactions" Kalghatgi, G., 2014 SAE International, Warrendale, Pa, ISBN 878-0-7680-6458-2

18. ASTM D4814-21, Standard Specification for Automotive Spark-Ignition Engine Fuel, Jan 12, 2021.

19. Wissink ML, Curran SJ, Roberts G, Musculus MP, Mounaïm-Rousselle C. Isolating the effects of reactivity stratification in reactivity-controlled compression ignition with iso-octane and n-heptane on a light-duty multi-cylinder engine. International Journal of Engine Research. 2018;19(9):907-926. doi:10.1177/1468087417732898

20. Dempsey, A, Curran, S, Wagner, R, & Cannella, W. "Effect of Premixed Fuel Preparation for Partially Premixed Combustion With a Low Octane Gasoline on a Light-Duty Multi-Cylinder Compression Ignition Engine." Proceedings of the ASME 2014 Internal Combustion Engine Division Fall Technical Conference. Volume 1: Large Bore Engines; Fuels; Advanced Combustion; Emissions Control Systems. Columbus, Indiana, USA. October 19–22, 2014. V001T03A012. ASME. https://doi.org/10.1115/ICEF2014-5561

21 Engine Emissions & Uncertainty Analysis, Dempsey, A., https://sourceforge.net/projects/engine-emissions-uncertainty/files/ [software] 2016

22 Moses-DeBusk, M., Curran, S.J., Lewis, S.A. et al. Impacts of Air-Fuel Stratification in ACI Combustion on Particulate Matter and Gaseous Emissions. Emiss. Control Sci. Technol. 5, 225–237 (2019). https://doi.org/10.1007/s40825-019-00122-5

23. Chuahy, F., DeBusk., M., Curran, S., Storey, J., "The effects of distillation characteristics and aromatic content on low-load gasoline compression ignition (GCI) performance and soot emissions in a multi-cylinder engine" Fuel, 2021,